Cloud Microphysical Properties Retrieved from Downwelling Infrared Radiance Measurements Made at Eureka, Nunavut, Canada (2006–09)

CHRISTOPHER J. COX

Department of Geography, University of Idaho, Moscow, Idaho

DAVID D. TURNER

NOAA/National Severe Storms Laboratory, Norman, Oklahoma

PENNY M. ROWE

Department of Geography, University of Idaho, Moscow, Idaho

MATTHEW D. SHUPE

Cooperative Institute for Research in Environmental Sciences, University of Colorado, and NOAA/Earth System Research Laboratory, Boulder, Colorado

VON P. WALDEN

Department of Geography, University of Idaho, Moscow, Idaho

(Manuscript received 14 March 2013, in final form 16 August 2013)

ABSTRACT

The radiative properties of clouds are related to cloud microphysical and optical properties, including water path, optical depth, particle size, and thermodynamic phase. Ground-based observations from remote sensors provide high-quality, long-term, continuous measurements that can be used to obtain these properties. In the Arctic, a more comprehensive understanding of cloud microphysics is important because of the sensitivity of the Arctic climate to changes in radiation. Eureka, Nunavut (80°N, 86°25′W, 10 m), Canada, is a research station located on Ellesmere Island. A large suite of ground-based remote sensors at Eureka provides the opportunity to make measurements of cloud microphysics using multiple instruments and methodologies. In this paper, cloud microphysical properties are presented using a retrieval method that utilizes infrared radiances obtained from an infrared spectrometer at Eureka between March 2006 and April 2009. These retrievals provide a characterization of the microphysics of ice and liquid in clouds with visible optical depths between 0.25 and 6, which are a class of clouds whose radiative properties depend greatly on their microphysical properties. The results are compared with other studies that use different methodologies at Eureka, providing context for multimethod perspectives. The authors' findings are supportive of previous studies, including seasonal cycles in phase and liquid particle size, weak temperature–phase dependencies, and frequent occurrences of supercooled water. Differences in microphysics are found between mixed-phase and single-phase clouds for both ice and liquid. The Eureka results are compared with those obtained using a similar retrieval technique during the Surface Heat Budget of the Arctic Ocean (SHEBA) experiment.

1. Introduction

Clouds play an important and complex role in the climate system by modulating the surface-energy budget. The net radiative forcing of clouds is caused by the interplay of albedo (negative forcing) and thermal emission (positive forcing) effects (Ramanathan et al. 1989), with the magnitude and sign being dependent on cloud properties. Properties including liquid and ice water paths, optical depth, temperature, particle size, and phase are important components of the radiative impact of clouds (e.g., Francis and Hunter 2007; Shupe and Intrieri 2004;

Corresponding author address: Christopher J. Cox, University of Idaho Geography Dept., McClure Hall 305B, Moscow, ID 83843.
E-mail: ccox@vandals.uidaho.edu

DOI: 10.1175/JAMC-D-13-0113.1

Sun and Shine 1994; Curry and Ebert 1992; Ebert and Curry 1992). Despite the importance of clouds, they are still considered a key uncertainty in our understanding of the climate system (Solomon et al. 2007).

Few measurements of cloud microphysics exist for the Arctic, partly because these types of measurements are difficult to obtain. Despite this observational limitation, previous research has shown that microphysical properties are linked to cloud processes. For instance, mixed-phase clouds are common in the Arctic and supercooled liquid has been identified in clouds at temperatures as low as 233 K (Shupe 2011; Shupe et al. 2006, 2008), but the relationship between cloud temperature and particle phase is still poorly understood (e.g., Shupe et al. 2008; Turner 2005). Significant cloud feedback mechanisms have been identified that are related to cloud water content, particle size, phase (Curry et al. 1996), and downwelling longwave radiation (Francis and Hunter 2007). Turner (2005) reports that the seasonal cycle in liquid droplet effective radii is likely related to seasonality in aerosols (e.g., Sirios and Barrie 1999), which have a climatologically significant impact on cloud emissivity (resulting in higher downwelling infrared fluxes) (Lubin and Vogelmann 2006; Garrett and Zhao 2006). Further, several studies have suggested that Arctic cloud microphysics are spatially nonuniform. De Boer et al. (2009) report significant differences in the microphysics between Barrow, Alaska, and Eureka, Nunavut, Canada. A similar finding has been reported when examining phase occurrence at a larger number of Arctic research stations (Shupe 2011).

Microphysical properties have been shown to be a critical component in cloud modeling (Vavrus 2004; Sun and Shine 1994). The need to characterize cloud microphysical properties in the Arctic has increased recently because the Arctic is exhibiting rapid environmental changes. These changes include melting permafrost (Romanovsky et al. 2010), decreases in sea ice extent (e.g., Wang and Overland 2009), changing boundary layer temperatures (Overland et al. 2008), spatial changes in downwelling longwave radiation (Francis and Hunter 2006), and changing cloud properties (Wang and Key 2005).

Several methods for determining cloud microphysics exist, including those from satellite observations (e.g., Kawamoto et al. 2001), in situ observations (e.g., Lawson et al. 2001), and ground-based observations (e.g., Garrett and Zhao 2013; Shupe 2007; Turner 2005; Matrosov et al. 2003; Frisch et al. 2002). Brief campaigns utilizing a broad range of measurement techniques, such as the Mixed-Phase Arctic Cloud Experiment (M-PACE) (Verlinde et al. 2007) and the Indirect and Semi-Direct Aerosol Campaign (ISDAC) (McFarquhar et al. 2011), have examined the role of microphysics in Arctic mixed-phase cloud processes. For instance, Verlinde et al. (2007) found that microphysical processes (notably, the mechanisms for ice formation) are important in maintaining supercooled liquid in mixed-phase clouds but are sensitive to changing synoptic conditions. Jackson et al. (2012) also found links between supercooled liquid and aerosols in ice nucleation within mixed-phase clouds.

Ground-based observations can provide long-term, continuous records of cloud microphysics to establish a baseline record of the types of microphysical conditions in the Arctic. This knowledge links process-oriented research to the Arctic climate system. Ground-based remote sensors including lidars, radar, microwave radiometers, and infrared spectrometers have been used to obtain cloud microphysics during the Surface Heat Budget of the Arctic Ocean (SHEBA; Uttal et al. 2002) experiment between 1997 and 1998 (Shupe et al. 2006, 2005; Turner 2005; Intrieri et al. 2002) and over land, including the North Slope of Alaska (Garrett and Zhao 2013; Shupe 2011; de Boer et al. 2009; Schofield et al. 2007; Verlinde et al. 2007; Wang et al. 2004; Dong and Mace 2003) and Eureka (Shupe 2011; de Boer et al. 2009; Bourdages et al. 2009). The various perspectives represented by ground-based remote sensors and the complexity involved in making retrievals yield differences in the results between retrieval algorithms (Zhao et al. 2012) and differences when compared to in situ observations (Vogelmann et al. 2012; de Boer et al. 2008; Turner 2007).

Here, we focus on microphysical properties retrieved from measurements of downwelling infrared radiation, which provide a unique perspective and are well suited for characterizing liquid water in clouds, thus helping to fill gaps in current knowledge (de Boer et al. 2009). To provide context for our results, we compare our results to those from previous studies that used different methodologies and provide qualitative discussion to help explain the similarities and differences. Characterizing liquid water is particularly important because the presence of liquid water in clouds strongly influences the radiative effect of the cloud (Bennartz et al. 2013; Cesana et al. 2012) and is poorly represented by climate models (Cesana et al. 2012; Liu et al. 2011). Cloud microphysical properties have previously been obtained using infrared radiances as a primary measurement over the Arctic Ocean during SHEBA (Turner 2005; Rathke et al. 2002a,b) and during the Arctic Ocean section in 1994 (Lubin and Simpson 1997). Retrieval of cloud microphysical properties from infrared radiation is particularly suited for improving understanding of infrared cloud radiative forcing because changes in spectral emission due to changes in cloud properties can be directly associated with changes in infrared flux. Microphysical properties

can be retrieved most accurately for clouds that have sufficient infrared signal and sufficient sensitivity to the microphysical properties themselves. In turn, these are the clouds for which understanding the microphysical properties is most important.

The microphysical properties presented here were obtained from infrared observations made from March 2006 through April 2009 at Eureka, Nunavut. In section 2, we describe the location and the instrumentation used in this study. In section 3, we discuss the retrieval algorithm used to obtain cloud microphysical properties. In section 4, we present the main results from this study. In section 5, these results are compared with results from similar measurements made during the SHEBA experiment. Conclusions are presented in section 6.

2. Experimental site and instrumentation

a. Location of study

Eureka, Nunavut (80°N, 86°25′W, 10 m), is a weather station run by Environment Canada and located on Ellesmere Island. Figure 1 shows a map of the study site. The instruments at Eureka that were used in this study were installed and operated by the Earth System Research Laboratory (ESRL) at the National Oceanic and Atmospheric Administration (NOAA) in conjunction with the Canadian Network for the Detection of Atmospheric Change (CANDAC) at the Zero Altitude Polar Environment Atmospheric Research Laboratory (PEARL) Auxiliary Laboratory (0PAL), which is located near sea level only 200 m from the Eureka Weather Station.

The seasonal cycle in temperature and humidity at Eureka was described by Cox et al. (2012) and is summarized as follows: 1) surface air temperatures at Eureka are strongly seasonally dependent and nearly always below freezing except in summer when the nearby fjord is melting; 2) December through March experience near-surface air temperatures below −30°C; 3) winter tropospheric temperatures (850–500 hPa) are typically warmer than near the surface (varying between −30° and −10°C) indicating the presence of a persistent temperature inversion layer; and 4) precipitable water vapor (PWV) also follows a strong seasonal cycle, peaking in July between 1.2 and 1.4 cm and becoming extremely low between November and March (~0.2 cm). Cloud characteristics at Eureka have been shown to be significantly different from other regions of the Arctic; the downwelling infrared flux at Eureka is low relative to most of the Arctic (Cox et al. 2012) and clouds at Eureka are thinner and higher relative to Barrow (de Boer et al. 2009).

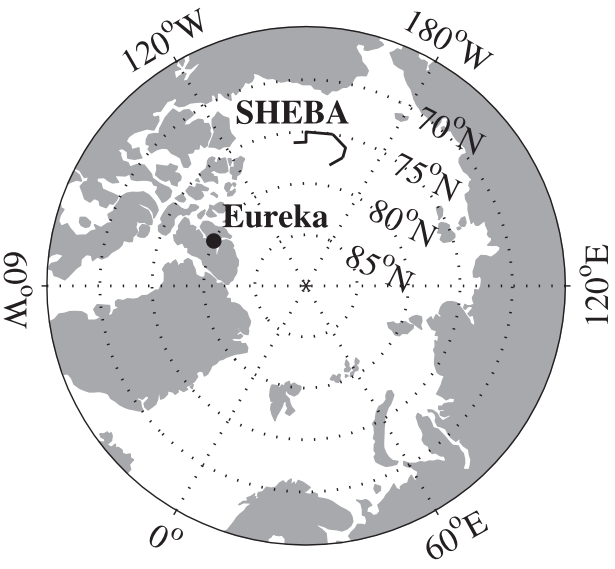

FIG. 1. Site location map. Eureka (80°N, 86°25′W, 10 m) and approximate SHEBA ship track are shown.

b. Infrared spectra

An Atmospheric Emitted Radiance Interferometer (AERI) was installed at Eureka in March 2006 and operated until April 2009. Since AERI observations are essential for the cloud microphysical retrievals presented here, this study is confined to the period of AERI operation, which was continuous except for a few short periods in June 2007, April 2008, and May 2008 when the instrument was being repaired. The AERI is a fully automated infrared spectrometer that is calibrated using two infrared reference sources; the overall accuracy is better than 1% of ambient radiance (Knuteson et al. 2004a,b). The AERI measures longwave radiance [$\mathrm{mW\,sr^{-1}\,m^{-2}\,(cm^{-1})^{-1}}$, hereinafter radiance units (RU)] at a high spectral ($0.5\,\mathrm{cm^{-1}}$) and temporal resolution (one spectrum every ~40 s) over a wavenumber range of 480–$3000\,\mathrm{cm^{-1}}$ (about 3–21 μm).

Spectral "microwindows" between strong gaseous emission lines are used in this study because they are sensitive to emission from clouds; a list is published in Table 1 of Turner (2005). Microwindows may contain more than one spectral data point so they can be averaged to reduce instrument noise. The radiance uncertainty associated with AERI measurements is generally less than about 0.2 RU across the majority of the spectrum (Knuteson et al. 2004a), but increases up to about 0.4 RU in the far infrared [~(480–550) $\mathrm{cm^{-1}}$] because the detector sensitivity drops off at low wavenumbers. Microwindows in the far infrared are used to determine cloud phase. Turner (2003, 2005) demonstrated a high degree of skill in cloud phase determination from

infrared spectra measured by the AERI; this study uses an improved version of the Turner (2005) method. The instrumental noise in the AERI spectra was reduced using a principal component technique (Antonelli et al. 2004; Turner et al. 2006).

During precipitation events at Eureka, a hatch closes over the AERI viewport to protect the optics, making data unusable. During the study period, the hatch was closed 16.1% of the time. All AERI spectra were quality controlled by considering the temperature stability of the reference sources, low instrument responsivity (an indicator of frost-covered optics), and excessive noise.

c. *Lidar and radar*

The Arctic High Spectral Resolution Lidar (AHSRL) (Eloranta 2005) and a Millimeter Cloud Radar (MMCR) (Moran et al. 1998) were operational at Eureka during the study period and collocated with the AERI. Cloud boundaries are provided to the retrieval algorithm by a combination of the radar and lidar measurements. The AHSRL measures profiles of backscatter and depolarization ratio at 2.5-s temporal and 7.5-m vertical resolution between 100 m and 30 km. The MMCR operates at both 45- and 90-m vertical resolutions between 100 m and 20 km and obtains profiles of reflectivity every 2 s.

d. *MWR*

Microwave radiometers (MWR) measure microwave emission from water vapor and liquid. A Radiometrics MP-1500 MWR is installed at Eureka; it takes measurements in 5 channels from 22 to 30 GHz at 15-s temporal resolution. From these measurements, retrievals of PWV and liquid water path (LWP) are obtained using two of the channels, 23.8 and 30 GHz (Turner et al. 2007). The PWV is used here for three purposes: 1) to scale the radiative transfer calculations of optical depth (see section 3b), 2) to screen for cases where the water vapor influence is large enough to cause unacceptable uncertainty in the microphysical retrieval, and 3) to provide supplementary information for the determination of LWP.

3. Retrieval algorithm

a. *MIXCRA*

The mixed-phase cloud retrieval algorithm (MIXCRA) (Turner 2005) is designed to estimate microphysical properties of both the ice and liquid components of a cloud using spectral infrared radiances supplemented with data from various instruments. A detailed description of the algorithm can be found in Turner (2005), but a description of how MIXCRA is used for this study is provided here.

Figure 2 shows a schematic of how the data from Eureka are used to produce retrievals of cloud properties, including references to sections of this paper that provide details of the processing steps. MIXCRA uses the observed downwelling infrared spectra with forward-model calculations performed using the Line-by-Line Radiative Transfer Model (LBLRTM), version 9.4 (Clough and Iacono 1995; Clough et al. 1992), and the combined LBLRTM and Discrete Ordinate Radiative Transfer model (DISORT) (LBLDIS; Turner 2005), version 4.13, to retrieve ice fraction, optical depth τ, particle effective radius, and ice and liquid water paths. (Infrared optical depth is retrieved at 900 cm^{-1} and converted to visible optical depth, which is reported in this paper.) The high-resolution transmission molecular absorption database (HITRAN) 2004 was used for the clear-sky radiance calculations (Rothman et al. 2005). LBLDIS combines clear-sky optical depth calculations from LBLRTM with the DISORT algorithm (Stamnes et al. 1988) to simulate radiance from a cloudy atmosphere.

The LBLRTM calculations require input of the vertical profiles of temperature and trace gases. These profiles are placed on a vertical grid of 47 levels between the surface and 17 km. The temperature and humidity profiles are obtained from Vaisala, Inc., RS-92 radiosondes launched twice daily by the Eureka Weather Station and were obtained from the Integrated Global Radiosonde Archive (IGRA; Durre et al. 2006); profiles that terminated below 17 km were supplemented with monthly-mean values. Because of a lack of measurements at Eureka, trace gas measurements of carbon dioxide (Conway et al. 2011), carbon tetrachloride (CCl_4), and chlorofluorocarbons F11 and F12 made at the surface at Barrow are used in each model atmosphere, assuming a constant mixing ratio; these data were observed at Barrow from 2006 through 2008 by the NOAA/ESRL Global Monitoring Division. The following trace gases were also included using the default concentrations for the sub-Arctic winter (McClatchey et al. 1972) in the LBLRTM model: ozone (O_3), nitrous oxide (N_2O), carbon monoxide (CO), and methane (CH_4). The contribution to the clear-sky radiative transfer from aerosols is not included in the calculations.

LBLRTM calculations of optical depth profiles were made at each radiosonde launch time. These profiles were then linearly interpolated in time to the AERI measurements. To account for a dry bias in the radiosonde humidity measurements (Turner et al. 2003; Rowe et al. 2008) and to better represent the change in water vapor between radiosondes, the optical depth profiles were then adjusted using the PWV from the MWR nearest in time to the each AERI measurement.

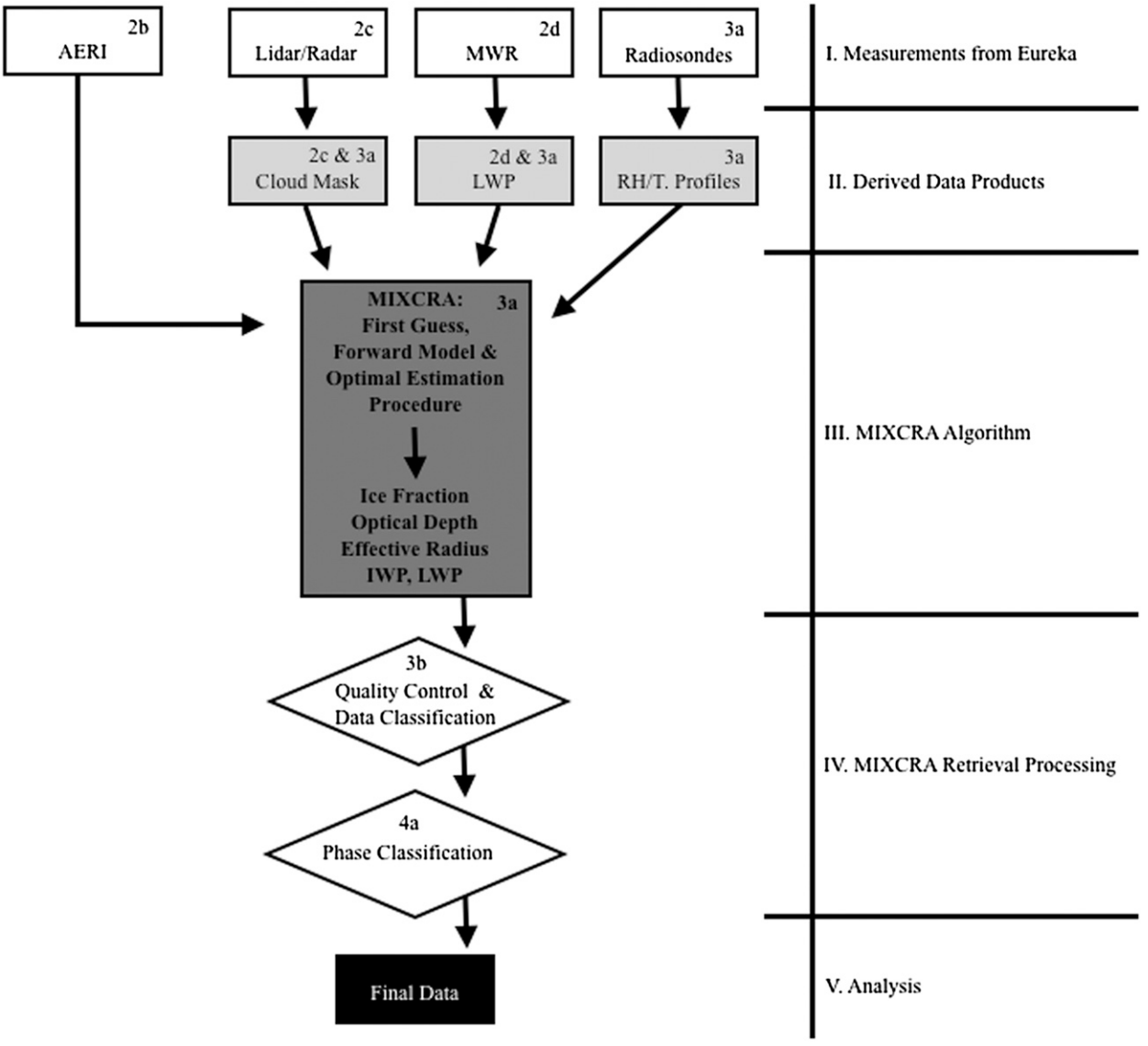

FIG. 2. Flowchart of the microphysical dataset acquisition procedure. White rectangles indicate measurements made at Eureka (I). Light gray rectangles indicate data products derived from the measurements (II). The dark gray rectangle is the MIXCRA algorithm (III). White diamond shapes indicate the processing of the MIXCRA retrieval (IV) including first quality control and data classification and then phase classification. The black rectangle (V) indicates the final dataset that is analyzed in this paper. The numbers in each box within the flowchart indicate the section of this paper where a detailed description can be found.

Liljegren and Lesht (1996) compared PWV derived from an MWR at the U.S. Department of Energy (DOE) Atmospheric Radiation Measurement Program (ARM) Southern Great Plains site in Oklahoma to PWV retrieved from the global positioning system (Rocken et al. 1995), finding a standard deviation of 0.11 cm in the differences. Retrieval uncertainties due to uncertainties in temperature and water vapor are minimized by using microwindows between strong lines of gaseous emission.

MIXCRA uses an iterative optimal estimation technique to find the best agreement between the simulated (LBLRTM and LBLDIS) and measured (AERI) radiances. The first-guess estimations of the cloud properties are made using a simple emissivity (ε) calculation at $900\,\mathrm{cm}^{-1}$ and assuming an ice fraction of 0.5 when the cloud temperature is between 233 and 273 K. The first guess for the effective radius is set to a reasonable value for Arctic clouds. The physical boundaries of the cloud are provided by a product determined from a combination of lidar and radar data. The MIXCRA LWP retrieval includes radiances from both the AERI and the MWR, further constraining the solution (Turner 2007).

During the first five months before the MWR was installed, retrievals were performed without the initial LWP from the MWR. During this time, only the AERI measurements were used to determine LWP, resulting in a larger uncertainty in the MIXCRA retrievals. Also during this time period, the PWV was calculated using only the radiosonde humidity profiles but interpolated to the AERI measurement times. Since the AERI cannot resolve cloud properties in the vertical, MIXCRA models all clouds as single layer. Turner and Eloranta (2008) have shown that the optical depth retrievals from MIXCRA agree well with those from lidar for single-layer mixed-phase clouds measured during M-PACE.

b. Data classification and quality control

To retrieve cloud microphysical properties from downwelling infrared emission spectra, the emission must be sensitive to changes in the cloud microphysics, and there must be adequate signal from the cloud. For the purposes of this work, we define thin clouds to be those with optical depths less than 0.25, intermediate clouds to have optical depths of 0.25–6, and thick clouds to have optical depths greater than 6. Clouds that are optically thin (e.g., τ in the visible $< \sim 0.25$, and ε at $900\,\mathrm{cm}^{-1} < \sim 0.1$) have low emission in the infrared, resulting in a small signal-to-noise ratio, and at some frequencies the cloud signal may also be small compared to the emission from atmospheric gases. Thus, uncertainties in the retrieved variables for thin clouds are large. Thick clouds ($\tau > \sim 6$, and $\varepsilon \sim 1$) emit significantly in the infrared, but because they behave like blackbodies, their infrared flux depends primarily on thermodynamic temperature with little sensitivity to microphysics. Clouds of intermediate optical thickness (e.g., $0.25 < \tau < 6$) have large signal to noise and are sensitive to cloud microphysical properties. In turn, this means that the radiative properties of intermediate-thickness clouds can be impacted by changes in microphysics that result from changes in atmospheric conditions, such as the meteorology or aerosol concentration. Thus, we restrict our analysis to intermediate-thickness clouds.

The sample that is analyzed in this paper is a subset of the AERI measurements. Furthermore, the optical depth thresholds for rejection of thin and thick clouds depend on the particular retrieved variable; thus, there are different sample sizes for different retrieved variables. To provide context for the samples that are analyzed throughout the paper and to estimate the frequency of occurrence of clouds at Eureka with intermediate optical depths, we classify the entire dataset into clear sky–thin clouds, thick clouds, and intermediate-optical-depth clouds. These classifications are shown in Fig. 3 for different variables.

Before discussing the classifications, we first discuss the parameters that were used to sort the data. MIXCRA can retrieve properties from clouds that have very low optical depths, but to avoid ambiguity as to whether a cloud is overhead, we set a conservative optical depth threshold (defined below) to delineate clear from cloudy conditions. In actuality, thin clouds are prevalent at Eureka (Cox et al. 2012), so a large fraction of clouds at Eureka have optical depths below our threshold. Thus, our approach here is conservative and provides high confidence that the analyzed scenes include clouds. Clouds are considered too thick when the total optical depth exceeds 6; most of the clouds rejected for this reason occurred from July through September (Fig. 3). If the cloud optical depth is lower than 6, the PWV may still be high preventing the retrieval of ice fraction due to opacity in the far infrared (Turner et al. 2003). Thus, a PWV threshold was set to 1 cm, resulting in rejection of some clouds of intermediate optical depths from June through August (Fig. 3). Clouds that were within the analysis range were subject to quality control procedures. MIXCRA quality assurance tests remove data that fall into three categories: 1) the RMS value between the observed and calculated radiance exceeds a threshold of 1.2 RU, 2) the MIXCRA retrieval is the same as the first-guess value, or 3) opacity in the far infrared prevents a determination of phase when the cloud temperature is between 233 and 273 K.

The initial dataset includes 1.87 million spectra measured by the AERI. About 9.4% of these spectra were removed during AERI quality control procedures before ingestion into MIXCRA (see section 2b). These rejected spectra are assumed to be uncorrelated with meteorological conditions and were not included in the classification. About 16.1% of the AERI spectra were measured when the hatch was closed. Since hatch closures typically occur during precipitation events, rejection of these data represent a climatological bias; these cases are considered thick clouds in our classification, but note that hatch closures can also occur in blowing snow conditions. The remaining 1.42 million spectra were ingested into MIXCRA. The MIXCRA retrievals were then sorted so that the results for intermediate optical thickness clouds could be analyzed.

Figure 3 summarizes the classifications as composite monthly proportions in six categories. Thin clouds are represented by blue, thick clouds are shown as shades of red, and clouds of intermediate optical depth are given as shades of green. The clouds of intermediate optical depth are subdivided into data that were 1) retained for analysis (dark green), 2) rejected because of failure of MIXCRA quality control procedures (medium green), and 3) rejected because the PWV > 1 cm (light green). The thick clouds are subdivided as 1) too thick for

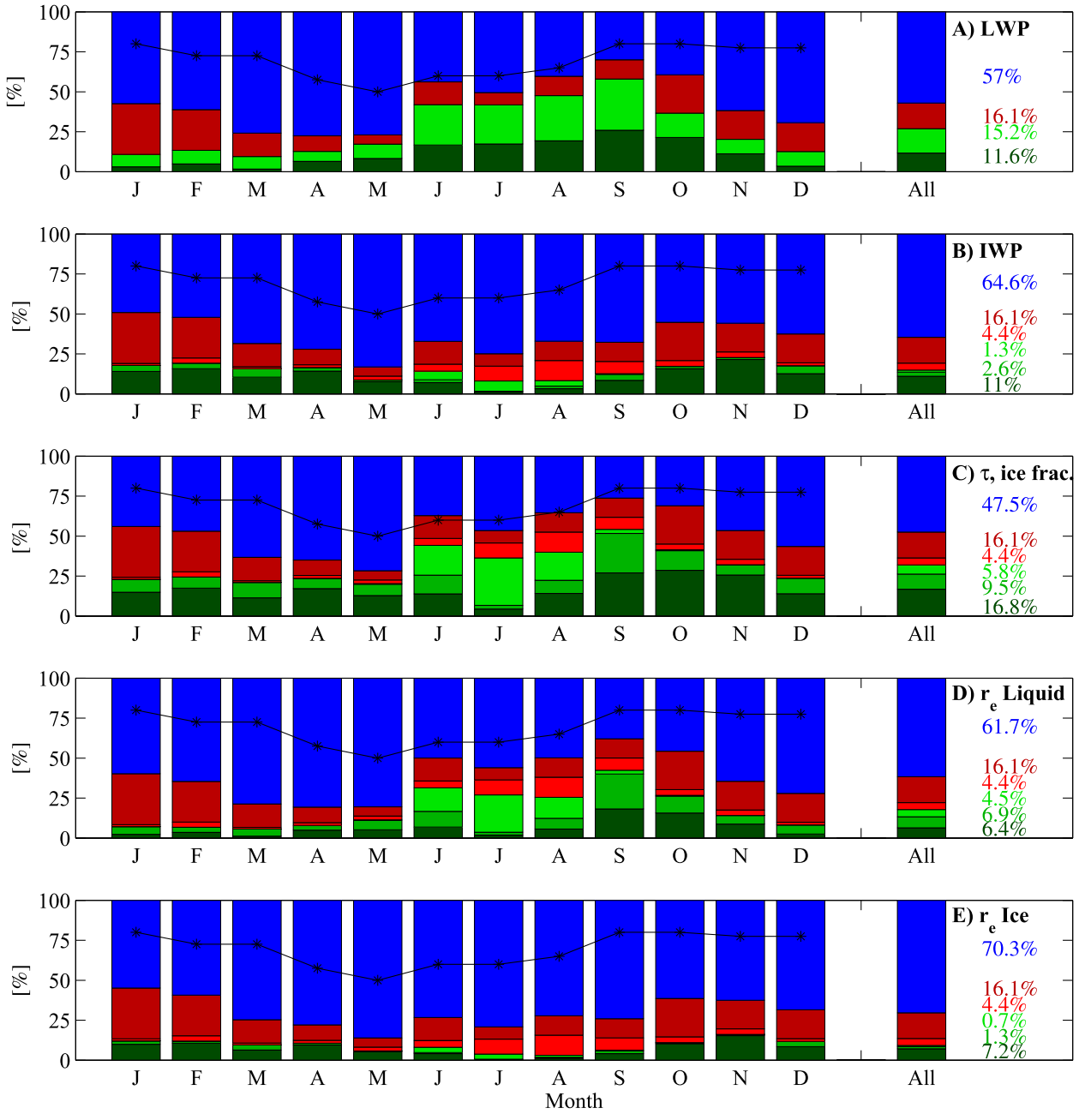

FIG. 3. MIXCRA retrieval data classification and quality control in 2006–09 monthly composites. The five plots represent the five final sample sizes that the retrieved variables fall into: (a) LWP, (b) IWP, (c) optical depth and phase, (d) liquid effective radius, and (e) ice effective radius; 100% of each bar graph in the all category represents about 1.87 million potential AERI measurements. Greens are clouds of intermediate optical thickness. reds are thick clouds; blues are thin clouds and clear sky. The greens are subdivided into samples that were retained for analysis (dark green), data that were rejected because the PWV was >1 cm (medium green), and data that were rejected because of failure of MIXCRA quality control procedures (light green). The reds are further subdivided in clouds that were too thick (light red) and AERI hatch closures (dark red). The black line is the approximate total cloud fraction from Fig. 2 in Shupe et al. (2011).

further analysis (rejected) (light red) and 2) AERI hatch closures (dark red). The clear-sky and thin clouds, which are considered together, are also rejected for further analysis and are shown as blue.

Figure 3a shows the classification percentages for the LWP ($N = 192\,278$). For LWP, the clear-sky threshold was set to a liquid optical depth of 0.25, but there was no upper limit set because the LWP also includes information

from the MWR, which is not limited by the infrared emissivity of the cloud. Figure 3b shows the percentages for the ice water path (IWP) ($N = 191\,975$). The IWP clear-sky threshold was set to an ice optical depth of 0.25 and the upper limits were set to $\tau = 6$ and PWV = 1 cm. Figure 3c shows the sample size for ice fraction (particle phase) and optical depth ($N = 289\,237$). These data were retained when $0.25 < \tau < 6$ and PWV < 1 cm. Figure 3d shows the classification percentages for liquid effective radius ($N = 108\,249$). These data were retained when the liquid optical depth was greater than 0.5, $\tau < 6$ and PWV < 1 cm. Figure 3e shows percentages for the ice effective radius ($N = 125\,303$). These data were retained when the ice optical depth fell between 0.5 and 5, $\tau < 6$ and the PWV < 1 cm. The more strict optical depth thresholds set for the effective radii retrievals is necessary because of sensitivity to the loss of spectral structure at low and high emissivities; see Turner (2005) for details.

The classification results shown in Fig. 3 set the context for meaningful interpretation of the data subsets that are analyzed in this study. Note that the approximate cloud fraction from Fig. 2 in Shupe et al. (2011) is overlaid on the bar graphs in Fig. 3; this cloud fraction is a composite monthly mean between August 2005 and September 2009 using multiple instruments. For each variable in Figs. 3a–e, the proportion of scenes classified as clouds (greens and reds) is well correlated with the cloud fraction from Shupe et al. (2011). The reason that our cloud fraction in Fig. 3 is lower than Shupe et al. (2011) is because our clear-sky classification includes thin clouds. Figures 3d and 3e include clouds up to an optical depth of 0.5 in the clear-sky and thin cloud category, so these figures show the largest biases in cloud fraction. The large increase in the proportion of scenes in the clear-sky and thin cloud category in these panels is an indication of the large proportion of clouds at Eureka with low optical depths. Note that in Fig. 3c, which contains the least number of clear sky–thin clouds in the clear-sky classification, the cloud fraction is similar to that of Shupe et al. (2011) in summer, suggesting that relatively few clouds at Eureka have optical depths below 0.25 during this time of year. An examination of the retained samples in Figs. 3a–e shows that the largest proportions of intermediate optical thickness clouds occur in the summer and autumn. The months with the highest percentage of samples retained for analysis occurred in the autumn because the proportion of clouds of intermediate optical depth is similar to the summer, but the PWV is typically lower.

Figure 4 shows histograms of the 3-h mean downwelling longwave cloud radiative forcing (DLCRF) from March 2006 through December 2008 (Cox et al. 2012) linearly interpolated to the times of the MIXCRA retrievals. [The DLCRF is a measurement of the downwelling infrared emission from the cloud but does not include the cloud's impact on the surface temperature, so it differs slightly from the conventional definition of cloud radiative forcing (see Shupe and Intrieri 2004).] The total DLCRF (black) in Fig. 4 is bimodal: high values are thick clouds and clear sky is centered around approximately zero (within the uncertainty of the measurement), but the clear-sky distribution probably includes many optically thin clouds. The values in the range between the thick cloud and clear-sky–thin cloud peaks are clouds of intermediate optical depth. The large sensitivity of these clouds to microphysical properties is evidenced by the increased variability in DLCRF of these clouds compared to the narrower clear-sky–thin cloud and thick cloud distributions. Figure 4 suggests that this range of radiative characteristics is well represented by all variable samples despite the fact that the samples are small.

Similarly to Fig. 4, recent studies have characterized the Arctic atmosphere into two distinct states: radiatively clear and opaquely cloudy (Cox et al. 2012; Morrison et al. 2012; Stramler et al. 2011). As shown in Fig. 4, the sample of clouds considered here are made up of the large number of clouds that exist between these states at Eureka (intermediate optical thicknesses), but we speculate are likely to be more representative of the meteorology of the cloudy state than the radiatively clear state. For Arctic mixed-phase stratiform clouds, which make up a large proportion of the clouds sampled in this study, the synoptic-scale pattern is responsible for the moisture, and therefore cloud generation (Morrison et al. 2012). At Eureka, this moisture likely comes from the south and west (Cox et al. 2012; de Boer et al. 2009). The maintenance and persistence of Arctic mixed-phase stratiform clouds is largely supported by local thermodynamic conditions via a number of buffering processes and feedbacks, whereas thicker clouds, which are not sampled here, are shorter lived, more transient, more energetic, and closely tied to the larger-scale dynamics (Morrison et al. 2012). We speculate that the thinnest clouds, which are also not sampled here, may be associated with orographic influence of the high elevations over the northern parts of Ellesmere Island under northerly winds, which are the predominant condition at Eureka (Cox et al. 2012).

4. Results and discussion

a. Ice fraction and cloud phase

Clouds with temperatures greater than 273 K are assumed to be liquid-only, and clouds with temperatures below 233 K are assumed to be ice-only. Between these

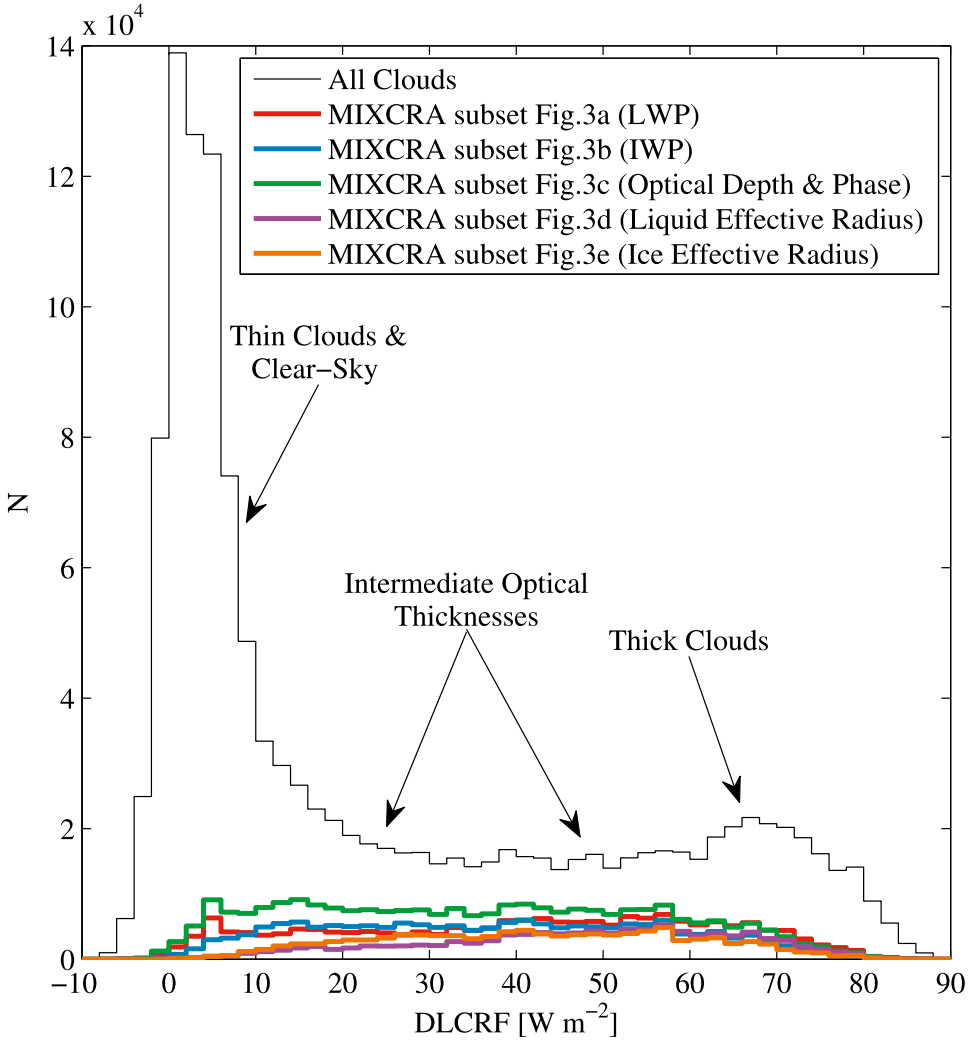

FIG. 4. Histograms of DLCRF interpolated to MIXCRA times for 2006–08 (Cox et al. 2012). Histograms of the subsamples reported in this paper are also shown.

temperatures, ice-only, supercooled liquid, or mixed-phase clouds may exist, and the optical depths of both the ice and liquid components of the cloud are retrieved using MIXCRA. The ice fraction is calculated from the optical depth retrieval as $f_i = \tau_i/(\tau_i + \tau_w)$; thus, the phase is a radiative classification (determined ultimately from the relative proportion of infrared emission from ice and liquid) rather than a physical classification. The cloud phase is then categorized from ice fraction using thresholds of $f_i = 0.02$ and 0.98 for liquid and ice, respectively; clouds with ice fractions between 0.02 and 0.98 are considered mixed phase.

Figure 5 shows the monthly classification of cloud phase determined by MIXCRA for March 2006 through April 2009 at Eureka from the cloud sample of intermediate optical depths (Fig. 3c). Averaged over the entire study period, 20% of these clouds are liquid only, 36% are mixed phase, and 44% are ice only. Mixed-phase clouds were a large proportion of the sample in all months (20%–70%) and represented the majority of clouds during the transition seasons (April, May, June, September, October, and November).

Shupe (2011) used multisensor observations (MMCR, AHSRL, MWR, and radiosondes) to report phase classifications at Eureka between August 2005 and October 2009. Note that the Shupe (2011) classification is a cloud fraction in time rather than a fraction derived only from times when clouds were present.

We find similar seasonal cycles in both ice and liquid clouds, but unlike Shupe (2011) who found a single mode in mixed phase, peaking in the autumn, we find a second peak in the spring. This peak indicates that at

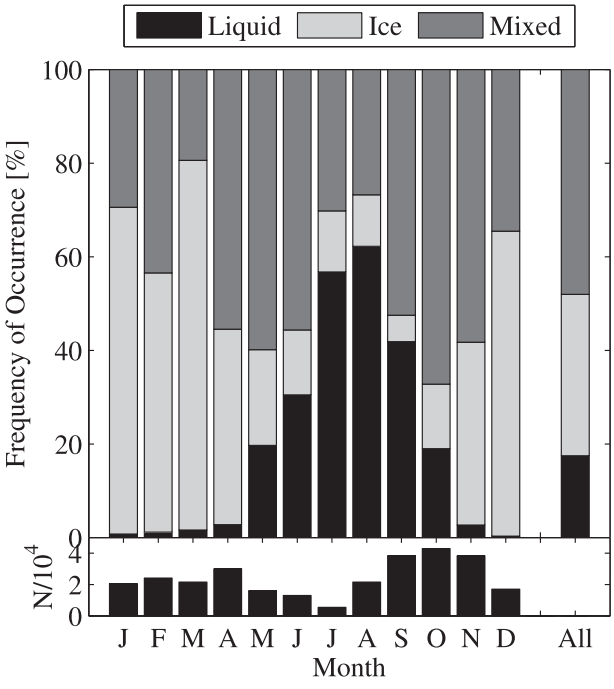

FIG. 5. Monthly-mean (2006–09 composite) phase classification as proportions of cloudy scenes for clouds with optical depths between 0.25 and 6.

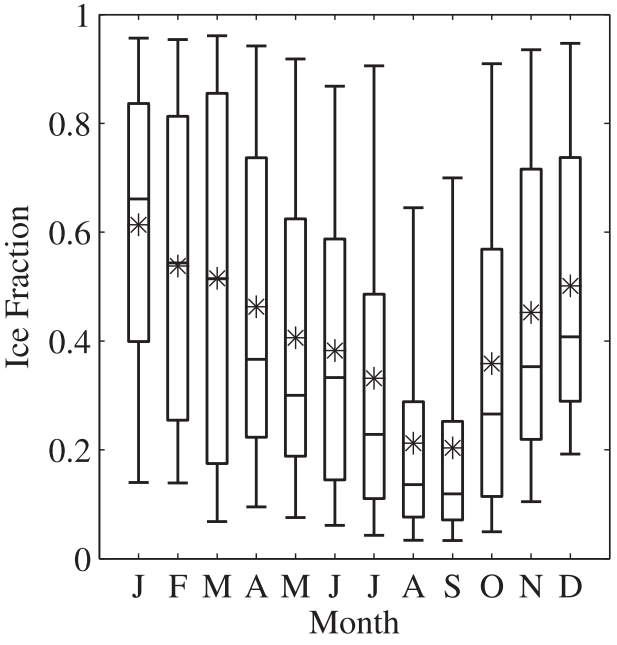

FIG. 6. Monthly (2006–09 composite) ice fractions for mixed-phase clouds with optical depths between 0.25 and 6. Shown are the 5%, 25%, 50%, 75%, and 95% percentiles and the mean (asterisk).

intermediate optical depths, infrared emission from liquid in mixed-phase clouds is important also in the spring, though the bimodal characteristic may be exaggerated: the decrease in summer mixed-phase clouds is likely influenced by subsampling as a result of the quality control, plus the absence of the spring peak in Shupe (2011) may be related to the Eureka cloud fraction minimum that also occurs in spring (Shupe et al. 2011). Similar to Shupe (2011), we find that liquid-only cloud occurrence is confined to the warm season with a peak in late summer. Figure 5 shows that for the clouds sampled here most are liquid only in July and August when the near-surface air temperatures are frequently above 0°C. However, if all clouds were considered, the proportion of liquid-only clouds would likely be lower for two reasons. First, in summer a larger number of mixed-phase clouds may be excluded because there are optical depths greater than the limit (see section 3b). Thick clouds are more likely to be mixed phase if we assume the formation process of Harrington et al. (1999), whereby clouds transition from liquid only to ice inclusion as they grow. Second, a large proportion of the thin clouds that were not analyzed (see section 3b) were likely cirrus (ice only). Between May and October, liquid is present in 80%–90% of the clouds sampled with a peak in August. Conversely, this proportion of liquid presence was only found in September by Shupe (2011). Qualitative analysis of AHSRL data for a sample of the small number of winter liquid-only classifications (<3%) confirms that there was significant liquid presence in those clouds, but it is important to reiterate that the phase classification is optical, not physical, and that the threshold for liquid only (0.98 ice fraction) could still contain a small amount (<2%) of ice. The MIXCRA retrievals of a single cloud system frequently include both mixed-phase and liquid-only classifications. This occurs in regions of a cloud where the signal from ice becomes too weak to detect.

Ice fraction in the mixed-phase intermediate optical thickness clouds is shown in Fig. 6. The mean follows a seasonal cycle and is less than 0.5 in most months. It peaks in January (0.6) and reaches a minimum in July and August (0.2). Ice clouds are the most prevalent phase between December and March (55%–80% of sampled clouds, Fig. 5).

Figure 7 shows contour plots of the annual cycle of the cloud occurrence of sampled clouds for all clouds (Fig. 7a), ice only (Fig. 7b), mixed phase (Fig. 7c), and liquid only (Fig. 7d). These plots are similar to the Eureka panels from Fig. 3 in Shupe (2011). Note that this paper uses the same cloud height data as Shupe (2011), but includes a different subset of clouds and a different retrieval method; see Shupe (2011) and Shupe et al. (2011) for a detailed explanation of the seasonal cycle in cloud heights. There are two significant differences between Fig. 7 and Shupe (2011). First, the cloud fraction derived

in this study is for times when a cloud was sampled by MIXCRA (Fig. 3c) rather than for all times. Second, our cloud fraction is derived assuming the cloud is centered between the lowest cloud base and the highest cloud top, even though in actuality there may have been multiple cloud layers. Despite these differences, Fig. 7 is qualitatively similar to the results from Shupe (2011). For instance, there is a general increase in the height of clouds and fewer low clouds during the summer, in particular for ice-only clouds.

There are also some key differences. First, as already discussed regarding Fig. 5, we find that the autumn peak in mixed-phase clouds is followed by a peak in spring. Figure 7c shows that the vertical distribution of the spring mixed-phase clouds is somewhat lower in the atmosphere than in the autumn. Finally, Fig. 7d shows the vertical distribution of liquid clouds. Similar to Shupe (2011), a peak below 2 km appears in the autumn for liquid-only clouds and these clouds are higher in the summer. It is likely that the high-altitude liquid-only classifications did actually contain some ice: our results indicate that these clouds were radiatively dominated by liquid, but the result may be complicated if multiple cloud layers were present in the scene.

b. *Cloud microphysics*

Statistics of MIXCRA retrievals of IWP, LWP, and effective radius of ice and liquid are presented in this section from the associated samples shown in Fig. 3. These quantities are reported, except where otherwise described, as box-and-whisker plots illustrating the mean and the 5%, 25%, 50%, 75%, and 95% percentiles.

IWP and LWP statistics are shown in Fig. 8 for single and mixed-phase clouds separately. IWP in ice-only clouds follows a seasonal cycle that peaks in the April (mean = $13\,\mathrm{g\,m^{-2}}$) and reaches a minimum in July (mean = $8\,\mathrm{g\,m^{-2}}$). IWP in mixed-phase clouds follows a similar seasonal cycle but is generally smaller (~30%) than in ice-only clouds. This pattern is consistent in all months except January (and even when the sample size is small). We report LWP (Fig. 8b) for all clouds with liquid optical depths greater than 0.25. The information provided by the AERI helps constrain the result at low values where LWP derived from an MWR alone has a large uncertainty (of order 20–$25\,\mathrm{g\,m^{-2}}$) (Turner 2007). However, LWP is still obtained by MIXCRA only when an AERI spectrum was measured; AERI hatch closures and MIXCRA quality control failures are not included so the sample size is relatively small, especially in summer. Therefore, for context, we have also plotted the mean LWP retrieved from the MWR (Turner et al. 2007) for all MIXCRA times (triangles) and for all times when an MWR observation was made regardless of whether an AERI measurement was made (circles) (note that circles represent LWP mean under all conditions, including clear sky). All LWP samples show similar seasonal cycles, peaking in September and a reaching a minimum in May. In months containing a large sample size of both liquid-only and mixed-phase clouds, the LWP in mixed-phase clouds is typically higher.

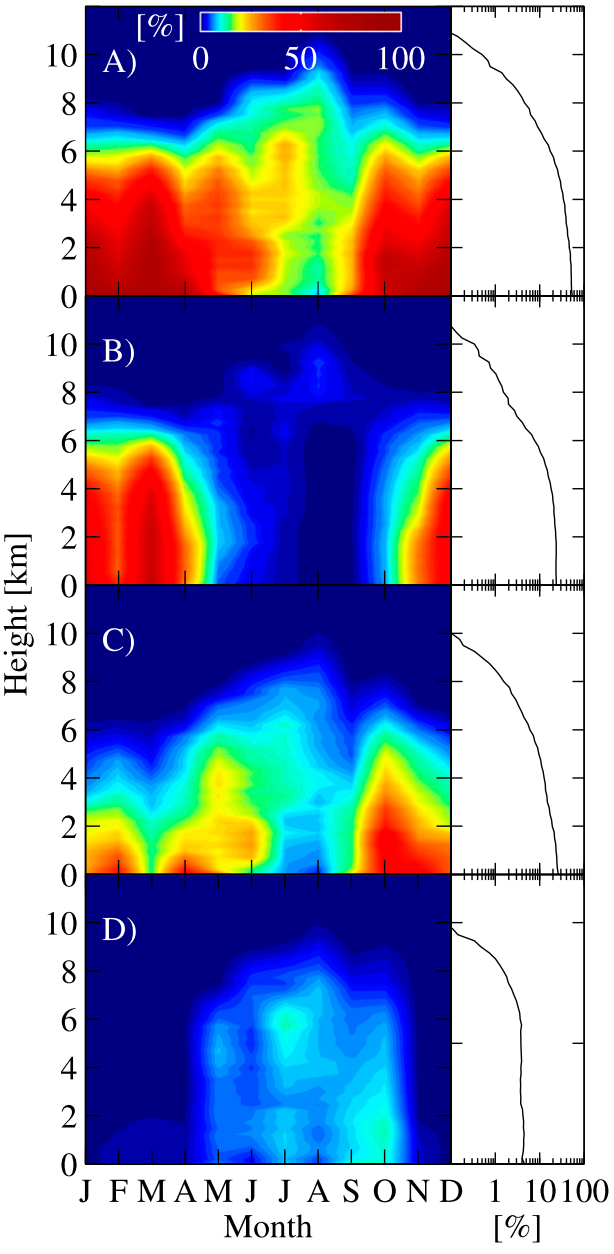

FIG. 7. Contour plot of cloud occurrence as a function of month and cloud height for clouds with optical depths between 0.25 and 6 for (a) all cloud phases together, (b) ice-only clouds, (c) mixed-phase clouds, and (d) liquid-only clouds. The color scale is base-10 logarithmic to emphasize low values of ice fraction. The curves to the right of the panels indicate the average for all months.

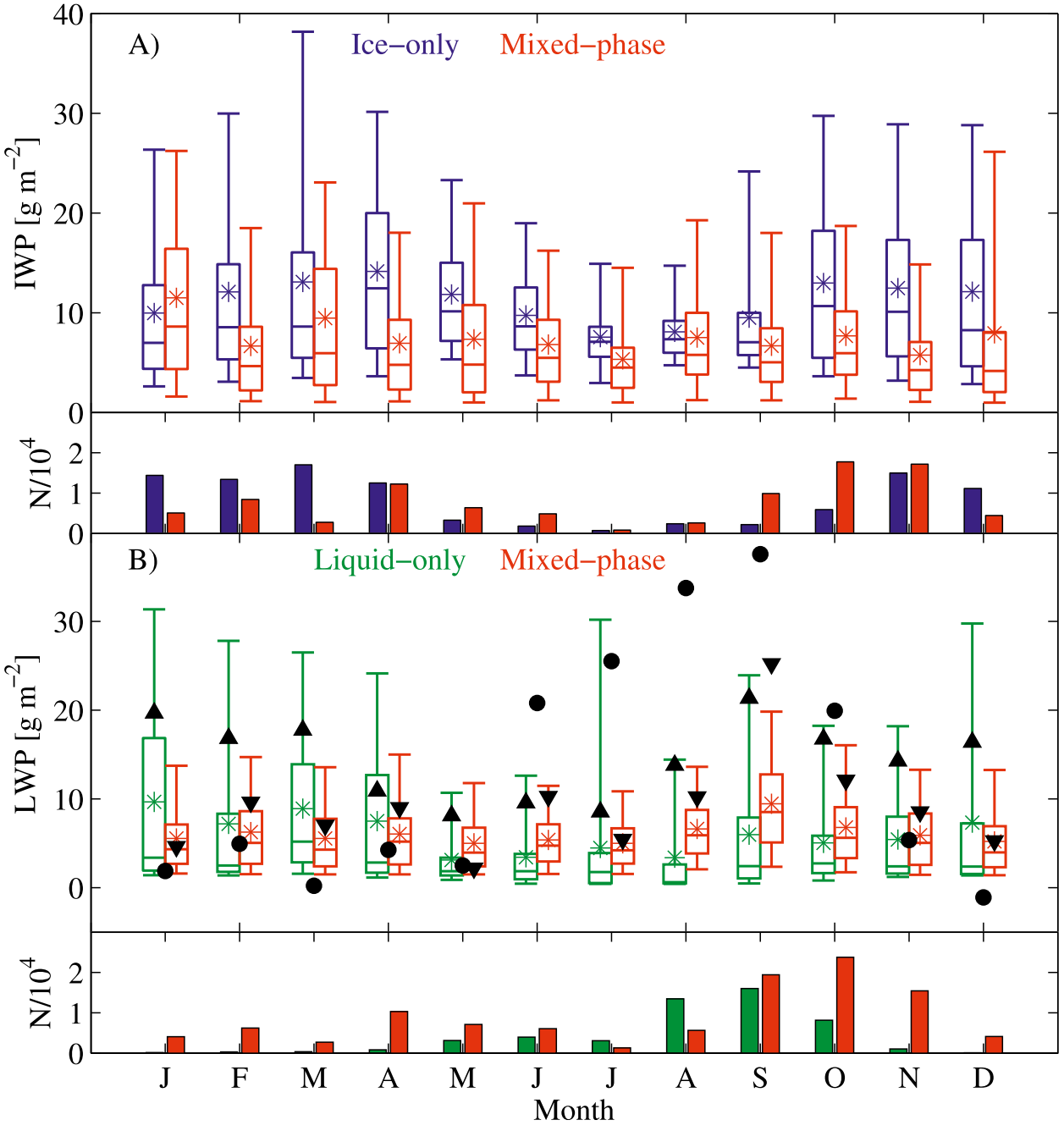

FIG. 8. Monthly distributions of IWP for clouds with ice optical depths between 0.25 and 6 and LWP for clouds with liquid optical depths > 0.25 (2006–09 composite). Each distribution illustrates the 5th, 25th, 50th, 75th, and 95th percentiles as a box-and-whisker plot. The asterisk denotes the mean value. LWP additional symbols are mean values of MWR LWP at MIXCRA times (triangles) and all MWR times (circles). Also shown are sample sizes N as bar plots.

Statistics of effective radius are shown in Fig. 9. The minimum ice effective radius was set in MIXCRA to 5 μm because this was the minimum size in the scattering properties database that was used by the retrieval; <6% of the mixed-phase clouds and <0.5% of ice-only clouds were retrieved below these minima. The effective radius of ice-only clouds (Fig. 9a) shows a slight seasonal cycle peaking in March (mean = 22 μm). A second peak of similar magnitude occurring in August may be a spurious result due to the small sample size. In other months, the ice effective radius distributions do not vary significantly. The effective radius of ice in mixed-phase clouds

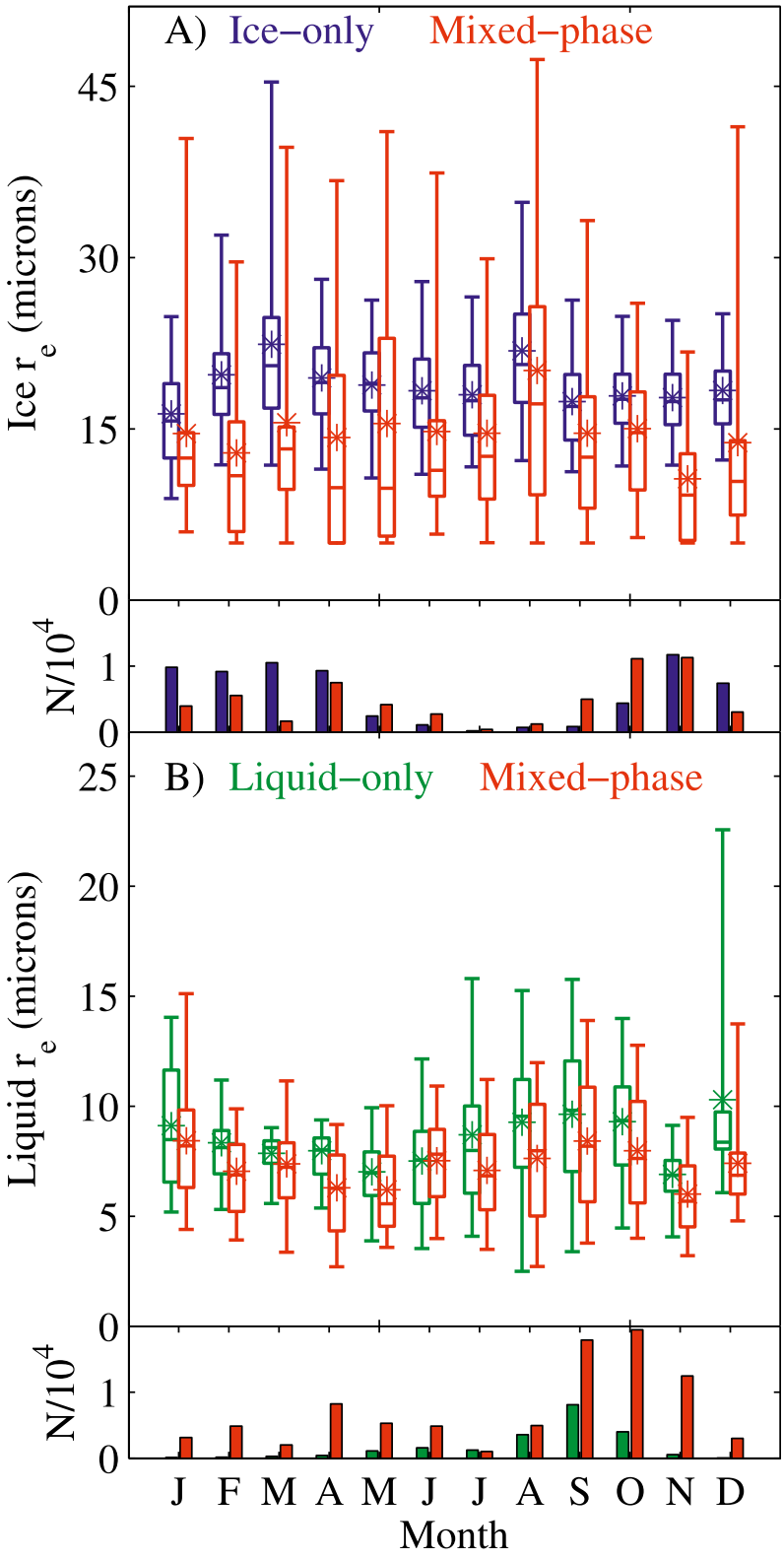

FIG. 9. Effective radius (μm) of (a) ice (for ice optical depths between 0.5 and 5 and total optical depth < 6) and (b) liquid (for liquid optical depth > 0.5 and total optical depth < 6). Each distribution illustrates the 5th, 25th, 50th, 75th, and 95th percentiles as a box-and-whisker plot. The asterisk denotes the mean value. Also shown are sample sizes N as bar plots.

does not vary dramatically with season, but is typically smaller (~20%) than in ice-only clouds. This was also observed by Turner (2005) in MIXCRA retrievals obtained during SHEBA. Since smaller effective radii of ice in mixed-phase clouds are counterintuitive (higher supersaturations over ice in mixed-phase conditions should produce more efficient ice growth and larger effective radii), we speculate that the result is related instead to the nature of the infrared retrieval. The individual components of complex crystal shapes, such as dendrites or aggregates that might be found in mixed-phase clouds, can produce a radiatively equivalent solution to multiple individual crystals of simpler habit that are assumed for the retrieval (Grenfell and Warren 1999); therefore the result is likely indicative of differences in ice habit rather than particle size between ice-only and mixed-phase clouds (Turner 2005).

Since liquid emits strongly in the infrared, and the shape of liquid droplets can be assumed to be spherical, infrared measurements are well suited for retrievals of liquid effective radius. The effective radius in liquid clouds (Fig. 9b) is consistently smaller than the effective radii of ice particles. The liquid droplet effective radius is 8–10 μm in most months but smaller in the spring (November may be a spurious result due to the small sample size). The trend is apparent in both liquid-only and mixed-phase classifications. This trend may be related to the seasonal cycle of aerosols in the Arctic (an increase in aerosol concentrations in the spring relative to other times of the year) that has been measured at Alert, Canada (on the northern tip of Ellesmere Island), by Sirios and Barrie (1999). These aerosols could impact the liquid effective radius over Eureka by providing a large source of condensation nuclei such that the liquid mass is distributed over a larger number droplets (Twomey 1977), thereby increasing cloud emissivity (Lubin and Vogelmann 2006; Garrett and Zhao 2006).

Liquid droplets in the mixed-phase clouds are observed to be smaller in size (~15%) than in liquid-only clouds. The correlation at the daily level is also apparent ($r \sim 0.8$) when mixed-phase and liquid-only classifications were both made (~32% of days May–September, ~19% overall). This observation supports the findings of Morrison et al. (2005) who determined through a 1D cloud model that contact freezing, favoring nucleation of larger liquid droplets, plays a dominant role in the persistence of mixed-phase clouds; the preferential freezing of these droplets changes the shape of the liquid water droplet size distribution, resulting in a smaller effective radius of water droplets. However, even though the results are consistent with this physical process, it may not be sufficient to explain such a large reduction in the liquid effective radius since the number of contact freezing events is likely very small compared to the total number of liquid droplets. Other explanations may be the Bergeron–Findeisen process, which retards or reverses the growth of liquid droplets in the presence of ice because of differences in the saturation vapor pressures over liquid and ice and that higher fall velocities associated with larger droplets may increase the probability of these droplets accreting ice.

Figure 10 shows temperature dependence of ice fraction and cloud optical depth as density plots similar to Turner (2005). These are based on the thermodynamic cloud temperature that was used for the MIXCRA retrieval and was produced from radiosonde profiles and lidar/radar cloud boundaries (Turner 2003). In this paper, only mixed-phase clouds are shown in Figs. 10c and 10d, but single-phase and mixed-phase clouds are shown together in Figs. 10a, 10b, and 10e. Only a very weak temperature dependence can be seen in Fig. 10a on optical depth ($r = 0.36$). The clouds in Fig. 10a that have temperatures greater than 273 K (liquid only) overwhelmingly have low optical depths (<0.6). This grouping extends from about 267 to 287 K. All of these cases occur from June through September (~17% of the total observations during this time) and are characteristic of clouds with low bases and physical thicknesses less than 300 m. The absence of warm liquid clouds with higher optical depths is likely due to the subsampling (which does not include optically thick clouds). Also, it is not an indication that liquid-only clouds of intermediate optical depth do not occur in summer because many of these were removed because of high PWV in summer (Fig. 3).

The temperature dependence of cloud phase in Arctic clouds has been examined by Turner (2005) and Shupe et al. (2006), where it is found that temperature alone does not determine phase. Similar to Shupe et al. (2006), we find that for mixed-phase clouds a slight negative correlation appears ($r = -0.44$, Fig. 10c) where ice fractions are somewhat lower in warm clouds. However, approximately 50% of mixed-phase clouds observed at Eureka are at temperatures below 250 K; this is a slightly cooler temperature than reported for Eureka by Shupe (2011), but recall that the clouds sampled by Shupe (2011) include thicker clouds, which are likely closer to the surface and therefore warmer. This temperature also approximately represents a transition from liquid dominated to ice dominated mixed-phase clouds (Fig. 10c). The liquid-only clouds sampled were also frequently supercooled (~75% of the clouds). From Fig. 10d, optically derived ice fraction in mixed-phase clouds indicates a liquid-dominated (low ice fraction) mixture.

The bimodal distribution in ice fractions less than 0.4 suggests two superimposed distributions. Separating these by season shows that the higher ice fraction peak

consists of winter values and the lower is from summer. Transition months are either more evenly distributed or also bimodal. This result may suggest that the abrupt shift in the thermodynamic state of the lower atmosphere at Eureka during the transition seasons (Cox et al. 2012) may be accompanied by a corresponding shift in cloud microphysics.

Overall distributions of effective radius and optical depth are arranged by phase in Fig. 11 in a manner similar to Fig. 9 in Turner (2005). Seasonality in optical depth results in a bimodal distribution of mixed-phase clouds. The thicker clouds of the upper mode occur throughout the year, but low optical depths are much more frequent during the cold months from October through June. In single-phase clouds, the mean effective radius of liquid droplets is 9 μm (with a standard deviation σ of 3 μm) and the mean effective radius of ice particles is 19 μm ($\sigma = 7\,\mu$m). In mixed-phase clouds, the mean effective radius of liquid droplets (7 μm; $\sigma = 3\,\mu$m) and ice particles (14 μm; $\sigma = 10\,\mu$m) are both smaller than in single-phase clouds. de Boer et al. (2009) report a mean effective radius of 10 μm for liquid droplets in mixed-phase stratiform clouds.

5. Comparison with MIXCRA results from SHEBA

Turner (2005) reported MIXCRA retrievals made during the SHEBA expedition between November 1997 and May 1998. Since these retrievals were obtained using the same algorithm as in this paper, they present an opportunity to compare retrievals from two different regions of the Arctic. The clouds that were sampled by Turner (2005) were subject to the same emissivity limitations as the clouds sampled for the present study. Therefore, the sample analyzed by Turner (2005) is similar to the sample analyzed in this study and a direct comparison is possible. Note that even though the same retrieval method is used, neither dataset represents a climatology, and the measurements do not overlap in time. For this comparison, we report only retrievals at Eureka from the same months examined by Turner (2005).

Liquid (ice) clouds are a smaller (larger) proportion of the sampled clouds at Eureka [4% (52%)] relative to SHEBA [20% (32%)]. Mixed-phase clouds at both locations are observed in more similar proportions (44% at Eureka, 48% at SHEBA). Shupe (2011) found larger proportions of both ice-only clouds and mixed-phase clouds at both locations and that nearly 2 times as many cloudy scenes contained mixed-phase clouds at SHEBA compared to Eureka. This inconsistency could be related to the subsampling of the present study, which likely removed a large number of ice-only clouds because they were optically thin, differences between the retrieval methods, higher optical depths in mixed-phase clouds at SHEBA (resulting in rejection from analysis), or because Turner (2005) used a more restrictive definition of mixed phase ($0.1 <$ ice fraction < 0.9) than we use here, resulting in fewer mixed-phase classifications. The modal ice fraction is smaller at Eureka (0.25) than at SHEBA (0.35).

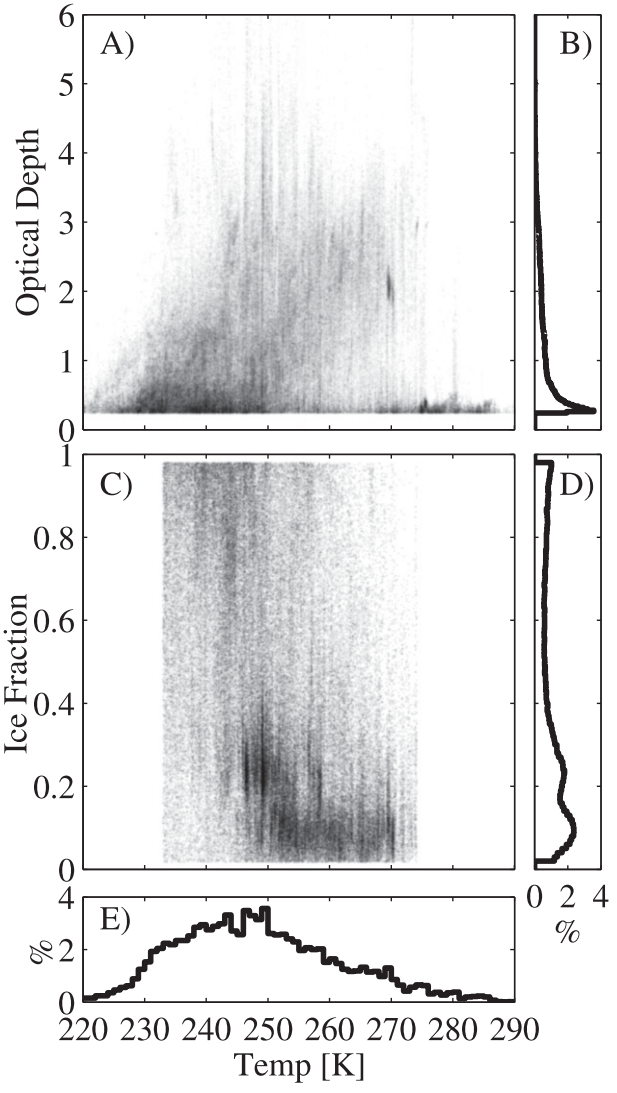

FIG. 10. Density plots for clouds with optical depths between 0.25 and 6. (a) Comparison of optical depth vs cloud temperature and (c) comparison of ice fraction vs cloud temperature for mixed-phase clouds. The shading is base-10 logarithmic. Histograms of (b) optical depth, (d) ice fraction in mixed-phase clouds, and (e) cloud temperature.

To facilitate comparison with Turner (2005), Fig. 12 shows similar distributions as in Fig. 11 but for only the months of November through May. Note that the sample of liquid-only observations is reduced considerably because of the months represented. The distribution of

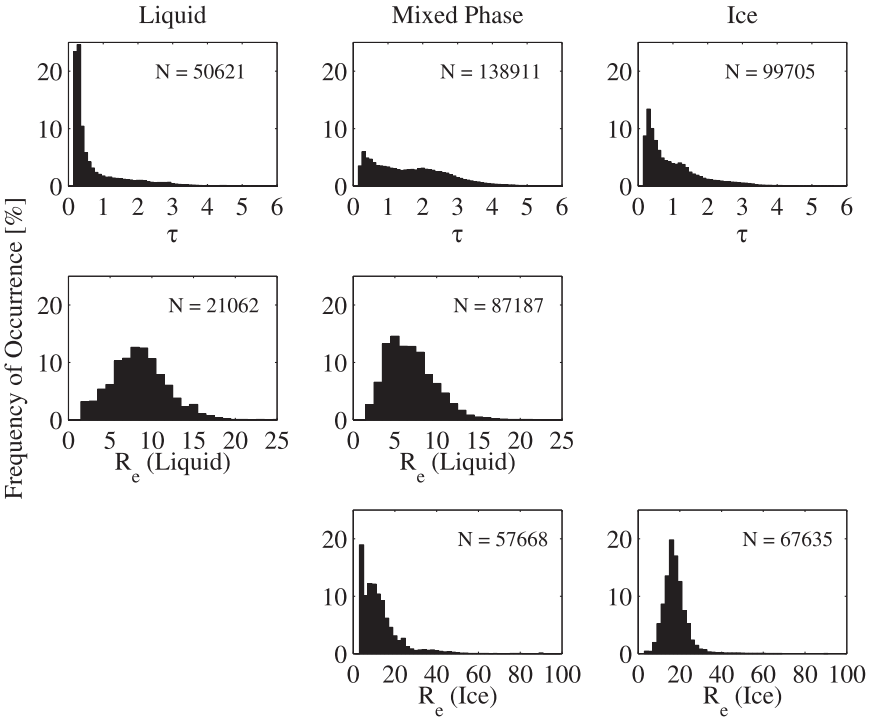

FIG. 11. The 2006–09 distributions of (top) optical depths between 0.25 and 6, (middle) effective radius with respect to liquid for liquid optical depth > 0.5 and total optical depth < 6, and (bottom) effective radius with respect to ice for ice optical depths between 0.5 and 5 and total optical depth < 6, arranged by phase.

liquid effective radii in mixed-phase clouds in Fig. 12 includes fewer high values than the annual distribution in Fig. 11. This is because most of the mixed-phase clouds in the November through May sample are from transition seasons (see Fig. 5) when the mean effective radii are smaller due to larger CCN concentrations (see section 4b). The optical depths of mixed-phase clouds are generally lower in the November through May sample than the annual distribution, as was discussed in section 4b.

Turner (2005) found effective radii in ice clouds to be distributed normally at lower values with a mode of 25 μm and a long tail of near-uniform distribution extending as high as 90 μm. At Eureka we also find a normally distributed particle size of ice clouds at lower values, but with a smaller mode of 17 μm (mean = 19 μm). A uniform distribution in particle sizes between 30 and 90 μm also occurs at Eureka, but the frequency of occurrence is less than 0.5%. Though modal droplet size in liquid clouds is similar at the two locations (9 μm), the variance is larger at SHEBA and many values occur that are greater than 15 μm. Turner (2005) reports that the monthly mode of effective radius in liquid clouds shifts from 10 μm in winter to 7 μm in spring, consistent with others in the western Arctic, and postulated a link between this observation and seasonality in aerosol concentration. As we showed in the previous section (Fig. 9b), a similar phenomenon occurs at Eureka.

Turner (2005) observed that increasing cloud temperatures from January through May did not cause a change in ice fraction distributions, but the time period represented in that study was short compared to the present study. At Eureka, where all months are represented, we find a significant seasonal cycle in ice fraction, including in the spring (Fig. 6). This can be partially explained by cloud temperature. Though the relationship between ice fraction and temperature is weak ($r = -0.44$; refer to section 4b), temperature does have some explanatory power. However, since the ice fractions reported here are radiative in origin, the seasonal cycles in effective radii also influence the ice fraction retrieval.

6. Conclusions

Many studies have shown that cloud microphysics play an important role in the radiative characteristics of clouds (e.g., Shupe and Intrieri 2004; Sun and Shine 1994; Ebert and Curry 1992; Curry and Ebert 1992) and are central to certain feedback mechanisms (Curry et al. 1996). Eureka, Canada, has been identified as

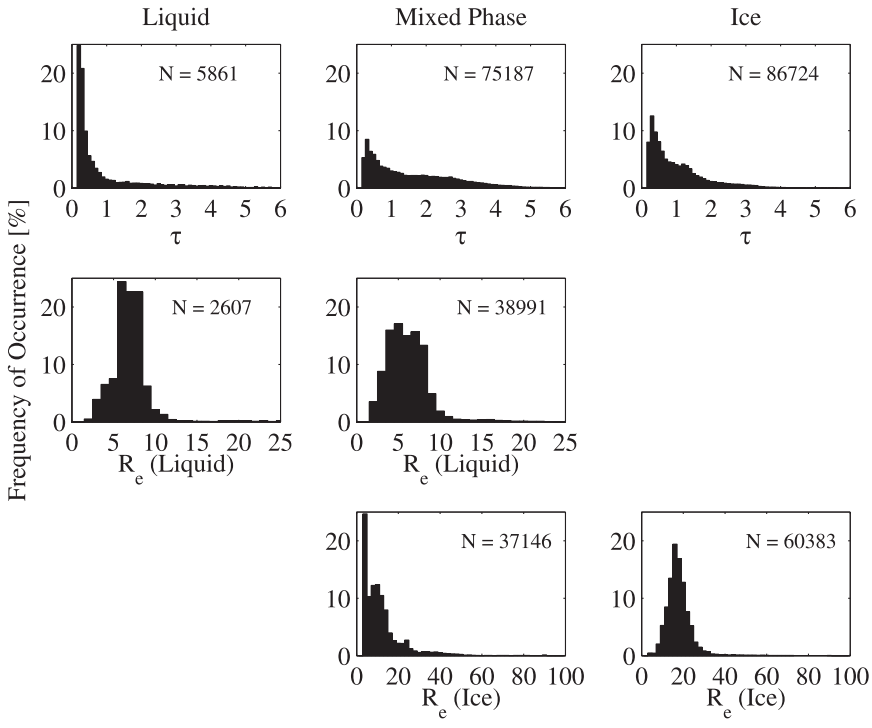

FIG. 12. As in Fig. 11, but for only November–May.

representative of a unique region of the Arctic with respect to cloud properties (Cox et al. 2012; Shupe 2011; Shupe et al. 2011; de Boer et al. 2009). This study expands the current knowledge of cloud microphysics to include infrared retrievals of mixed- and single-phase clouds of intermediate optical depths ($0.25 < \tau < 6$) at Eureka, and represents the longest retrieval record to date in the Arctic of cloud optical depth, phase, and effective radius. While the infrared emission of thick clouds is mainly dependent on temperature, the infrared emission of clouds of intermediate optical depth is also sensitive to cloud microphysical properties, including optical depth, particle effective radius, and thermodynamic phase. It is this sensitivity that enables retrieval of microphysical properties from infrared emission. Since clouds of intermediate thickness are an important part of the radiative budget, knowledge of their microphysical properties is crucial for improving weather and climate modeling and infrared remote sensing from satellites.

We compare our estimates of cloud microphysics and optical properties retrieved from passive infrared measurements to retrievals of microphysics obtained from different cloud samples at Eureka using methodologies that rely on lidar and radar observations reported in Shupe (2011) and de Boer et al. (2009). The results shown here are qualitatively consistent with these studies. This study provides valuable context for multimethod perspectives, which is needed for a more complete understanding of cloud microphysical properties. Long-term validations of all methods for microphysical retrievals from remotely sensed measurements using in situ observations are needed.

Our retrievals from infrared measurements show that the proportion of clouds of intermediate optical depths that are mixed phase is large in all months and dominates during the transition seasons in spring and fall. Like previous studies, we find mixed-phase clouds at temperatures down to 233 K and that cloud temperature is only weakly related to ice fraction (phase). About half of the mixed-phase clouds observed occurred at cloud temperatures below 250 K. Ice fractions (defined as the ratio of ice optical depth to total optical depth) in mixed-phase clouds are between 0.5 and 0.6 from December through March, are less than 0.5 in all other months, and exhibit a seasonal cycle that reaches a minimum of 0.2 in August and September. This large seasonal difference appears as separate modes of the overall distribution, possibly related to the large and rapid transition in temperature and water vapor between summer and winter at Eureka.

The ice water path peaks in the spring and is consistently larger in ice-only clouds; liquid water path peaks in September. The effective radii of ice are smaller in mixed-phase clouds than in ice-only clouds, an observation that is likely due to differences in habit rather than size. The effective radii of liquid droplets are also observed to be

smaller in mixed-phase clouds compared to liquid-only clouds. The mechanisms controlling this result may be a combination of the Bergeron–Findeisen process slowing the growth of liquid in mixed-phase clouds and preferential scavenging of the larger droplets by contact freezing, which is thought to be a necessary glaciation process in maintaining mixed-phase clouds (Morrison et al. 2005).

We compare the Eureka results with previous microphysical retrievals using the same method at SHEBA (Turner 2005) to gain an understanding of cloud microphysical properties across the greater Arctic region. Similar to Turner (2005), our retrievals from infrared measurements show evidence that the seasonal cycle of aerosols in the Arctic impacts the seasonal cycle of effective radius in liquid clouds. Liquid-only clouds were less frequent between November and May relative to SHEBA, but the frequency of mixed-phase clouds was similar. Ice fractions at Eureka were smaller than those observed at SHEBA.

Acknowledgments. This research was supported by National Science Foundation Grants ANS 0632177, ARC 0632187 and ARC 0856773, by Idaho's Experimental Program to Stimulate Competitive Research (EPSCoR) (NSF EPS 0814387), and by the Department of Energy Atmospheric Systems Research (ASR) program (Grants DE-FG02-06ER64167, DE-SC0008830, and DE-SC0007005). All measurements from Eureka were supported by the NOAA Earth System Research Laboratory (ESRL) Physical Sciences Division, with special thanks to Taneil Uttal. We are grateful to the Canadian Network for the Detection of Atmospheric Change (CANDAC) technicians for operating the instruments at Eureka from March 2006 through April 2009 and to the Environment Canada Weather Station at Eureka for their support. Additional observational data used in this study were provided by NOAA ESRL Global Monitoring Division (Pieter P. Tans, Jim Elkins, Jim Butler, Steve Montzka, and Thayne Thompson) and the Integrated Global Radiosonde Archive (IGRA). Computational support was provided by the Space Science and Engineering Center (SSEC) of the University of Wisconsin—Madison. We are thankful for comments from anonymous reviewers, which helped improve the manuscript.

REFERENCES

Antonelli, P., and Coauthors, 2004: A principal component noise filter for high spectral resolution infrared measurements. *J. Geophys. Res.,* **109,** D23102, doi:10.1029/2004JD004862.

Bennartz, R., and Coauthors, 2013: July 2012 Greenland melt extent enhanced by low-level liquid clouds. *Nature,* **496,** 83–86.

Bourdages, L., T. J. Duck, G. Lesins, J. R. Drummond, and E. W. Eloranta, 2009: Physical properties of high Arctic tropospheric particles during winter. *Atmos. Chem. Phys.,* **9,** 6881–6897.

Cesana, G., J. E. Kay, H. Chepfer, J. M. English, and G. de Boer, 2012: Ubiquitous low-level liquid-containing Arctic clouds: New observations and climate model constraints from *CALIPSO*-GOCCP. *Geophys. Res. Lett.,* **39,** L20804, doi:10.1029/2012GL053385.

Clough, S. A., and M. J. Iacono, 1995: Line-by-line calculation of atmospheric fluxes and cooling rates: 2. Application to carbon dioxide, ozone, methane, nitrous oxide, and the halocarbons. *J. Geophys. Res.,* **100** (D8), 16 519–16 535.

——, ——, and J.-L. Moncet, 1992: Line-by-line calculations of atmospheric fluxes and cooling rates: Application to water vapor. *J. Geophys. Res.,* **97** (D14), 15 761–15 785.

Conway, T. J., P. M. Lang, and K. A. Masarie, cited 2011: Atmospheric carbon dioxide dry air mole fractions from the NOAA ESRL Carbon Cycle Cooperative Global Air Sampling Network, 1968–2010. [Available online at ftp://ftp.cmdl.noaa.gov/ccg/co2/flask/month/.]

Cox, C. J., V. P. Walden, and P. M. Rowe, 2012: A comparison of atmospheric conditions at Eureka, Canada, and Barrow, Alaska (2006–2008). *J. Geophys. Res.,* **117,** D12204, doi:10.1029/2011JD017164.

Curry, J. A., and E. E. Ebert, 1992: Annual cycle of radiation fluxes over the Arctic Ocean: Sensitivity to cloud optical properties. *J. Climate,* **5,** 1267–1280.

——, W. B. Rossow, R. Randall, and J. L. Schramm, 1996: Overview of Arctic cloud radiation characteristics. *J. Climate,* **9,** 1731–1764.

de Boer, G., G. J. Tripoli, and E. W. Eloranta, 2008: Preliminary comparison of CloudSAT-derived microphysical quantities with ground-based measurements for mixed-phase cloud research in the Arctic. *J. Geophys. Res.,* **113,** D00A06, doi:10.1029/2008JD010029.

——, E. W. Eloranta, and M. D. Shupe, 2009: Arctic mixed-phase stratiform cloud properties from multiple years of surface-based measurements at two high-latitude locations. *J. Atmos. Sci.,* **66,** 2874–2887.

Dong, X., and G. G. Mace, 2003: Arctic stratus cloud properties and radiative forcing derived from ground-based data collected at Barrow, Alaska. *J. Climate,* **16,** 445–461.

Durre, I., R. S. Vose, and D. B. Wuertz, 2006: Overview of the integrated global radiosonde archive. *J. Climate,* **19,** 53–68.

Ebert, E. E., and J. A. Curry, 1992: A parameterization of ice cloud optical properties for climate models. *J. Geophys. Res.,* **97** (D4), 3831–3836.

Eloranta, E. W., 2005: High spectral resolution lidar. *Lidar: Range-Resolved Optical Remote Sensing of the Atmosphere,* C. Weitkamp, Ed., Springer-Verlag 143–163.

Francis, J. A., and E. Hunter, 2006: New insight into the disappearing Arctic sea ice. *Eos, Trans. Amer. Geophys. Union,* **87,** 509–511.

——, and ——, 2007: Changes in the fabric of the Arctic's greenhouse blanket. *Environ. Res. Lett.,* **2,** 045011, doi:10.1088/1748-9326/2/4/045011.

Frisch, S., M. D. Shupe, I. Djalalova, G. Feingold, and M. Poellot, 2002: The retrieval of stratus cloud droplet effective radius with cloud radars. *J. Atmos. Oceanic Technol.,* **19,** 835–842.

Garrett, T. J., and C. Zhao, 2006: Increased Arctic cloud longwave emissivity associated with pollution from mid-latitudes. *Nature,* **440,** 787–789.

——, and ——, 2013: Ground-based remote sensing of thin clouds in the Arctic. *Atmos. Meas. Tech.,* **6,** 1227–1243.

Grenfell, T., and S. G. Warren, 1999: Representation of nonspherical ice particle by a collection of independent spheres for scattering and absorption of radiation. *J. Geophys. Res.,* **104,** 31 697–31 709.

Harrington, J. Y., T. Reisin, W. R. Cotton, and S. M. Kreidenweis, 1999: Cloud resolving simulations of Arctic stratus: Part II: Transition-season clouds. *Atmos. Res.,* **51,** 45–75.

Intrieri, J. M., M. D. Shupe, T. Uttal, and B. J. McCarty, 2002: An annual cycle of Arctic cloud characteristics observed by radar and lidar at SHEBA. *J. Geophys. Res.,* **107** (C10), 8030, doi:10.1029/2000JC000423.

Jackson, R. C., and Coauthors, 2012: The dependence of ice microphysics on aerosol concentration in arctic mixed-phase stratus clouds during ISDAC and M-PACE. *J. Geophys. Res.,* **117,** D15207, doi:10.1029/2012JD017668.

Kawamoto, K., T. Nakajima, and T. Y. Nakajima, 2001: A global determination of cloud microphysics with AVHRR remote sensing. *J. Climate,* **14,** 2054–2068.

Knuteson, R. O., and Coauthors, 2004a: Atmospheric emitted radiance interferometer. Part I: Instrument design. *J. Atmos. Oceanic Technol.,* **21,** 1763–1776.

——, and Coauthors, 2004b: Atmospheric emitted radiance interferometer. Part II: Instrument performance. *J. Atmos. Oceanic Technol.,* **21,** 1777–1789.

Lawson, R. P., B. A. Baker, and C. G. Schmitt, 2001: An overview of microphysical properties of Arctic clouds observed in May and July 1998 during FIRE ACE. *J. Geophys. Res.,* **106** (D14), 14 989–15 014.

Liljegren, J. C., and B. M. Lesht, 1996: Measurements of integrated water vapor and cloud liquid water from Microwave Radiometers at the DOE ARM Cloud and Radiation Testbed in the U.S. Southern Great Plains. *Proc. IGARSS 1996,* Lincoln, NE, IEEE, 1675–1677.

Liu, X., and Coauthors, 2011: Testing cloud microphysics parameterizations in NCAR CAM5 with ISDAC and M-PACE observations. *J. Geophys. Res.,* **116,** D00T11, doi:10.1029/2011JD015889.

Lubin, D., and A. S. Simpson, 1997: Measurement of surface radiation fluxes and cloud optical properties during the 1994 Arctic Ocean Experiment. *J. Geophys. Res.,* **102** (D4), 4275–4286.

——, and A. M. Vogelmann, 2006: A climatologically significant aerosol longwave indirect effect in the Arctic. *Nature,* **439,** 453–456.

Matrosov, S. Y., M. D. Shupe, A. J. Heymsfield, and P. Zuidema, 2003: Ice cloud optical thickness and extinction estimates from radar measurements. *J. Appl. Meteor.,* **42,** 1584–1597.

McClatchey, R. A., R. W. Fenn, J. E. A. Selby, F. E. Volz, and J. S. Garing, 1972: Optical properties of the atmosphere. 3rd ed. Tech. Rep. AFCRL-72-0497, Air Force Geophysical Laboratories, 108 pp.

McFarquhar, G. M., and Coauthors, 2011: Indirect and semi-direct aerosol campaign: The impact of Arctic aerosols on clouds. *Bull. Amer. Meteor. Soc.,* **92,** 183–201.

Moran, K. P., B. E. Martner, M. J. Post, R. A. Kropfli, D. C. Welsh, and K. B. Widener, 1998: An unattended cloud-profiling radar for use in climate research. *Bull. Amer. Meteor. Soc.,* **79,** 443–455.

Morrison, H., M. D. Shupe, J. A. Pinto, and J. A. Curry, 2005: Possible roles of ice nucleation mode and ice nuclei depletion in the extended lifetime of Arctic mixed-phase clouds. *Geophys. Res. Lett.,* **32,** L18801, doi:10.1029/2005GL023614.

——, G. de Boer, G. Feingold, J. Harrington, M. D. Shupe, and K. Sulia, 2012: Resilience of persistent Arctic mixed-phase clouds. *Nat. Geosci.,* **5,** 11–17.

Overland, J. E., M. Wang, and S. Salo, 2008: The recent Arctic warm period. *Tellus,* **60A,** 589–597.

Ramanathan, V., R. D. Cess, E. F. Harrison, P. Minnis, B. R. Barkstrom, E. Ahmad, and D. Hartman, 1989: Cloud-radiative forcing and climate: Results from the Earth Radiation Budget Experiment. *Science,* **243,** 57–63.

Rathke, C., J. Fischer, S. Neshyba, and M. Shupe, 2002a: Improving IR cloud phase determination with 20 microns spectral observations. *Geophys. Res. Lett.,* **29,** doi:10.1029/2001GL04594.

——, S. Neshyba, M. D. Shupe, P. Rowe, and A. Rivers, 2002b: Radiative and microphysical properties of Arctic stratus clouds from multiangle downwelling infrared radiances. *J. Geophys. Res.,* **107,** 4703, doi:10.1029/2001JD001545.

Rocken, C., T. Van Hove, J. Johnson, F. Solheim, and R. Ware, 1995: GPS/STORM—GPS sensing of atmospheric water vapor for meteorology. *J. Atmos. Oceanic Technol.,* **12,** 486–478.

Romanovsky, V. E., S. L. Smith, and H. H. Christiansen, 2010: Permafrost thermal state in the polar Northern Hemisphere during the International Polar Year 2007–2009: A synthesis. *Permafrost Periglacial Processes,* **21,** 106–116.

Rothman, L. S., and Coauthors, 2005: The HITRAN 2004 molecular spectroscopic database. *J. Quant. Spectrosc. Radiat. Transfer,* **96,** 139–204.

Rowe, P. M., L. M. Miloshevich, D. D. Turner, and V. P. Walden, 2008: Dry bias in Vaisala RS90 radiosonde humidity profiles over Antarctica. *J. Atmos. Oceanic Technol.,* **25,** 1529–1541.

Schofield, R., and Coauthors, 2007: Retrieval of effective radius and liquid water path from ground-based instruments: A case study at Barrow, Alaska. *J. Geophys. Res.,* **112,** D21203, doi:10.1029/2007JD008737.

Shupe, M. D., 2007: A ground-based multisensor cloud phase classifier. *Geophys. Res. Lett.,* **34,** L22809, doi:10.1029/2007GL031008.

——, 2011: Clouds at Arctic atmospheric observatories. Part II: Phase characteristics. *J. Appl. Meteor. Climatol.,* **50,** 645–661.

——, and J. M. Intrieri, 2004: Cloud radiative forcing of the Arctic surface: The influence of cloud properties, surface albedo, and solar zenith angle. *J. Climate,* **17,** 616–628.

——, T. Uttal, and S. Y. Matrosov, 2005: Arctic cloud microphysics retrievals from surface-based remote sensors at SHEBA. *J. Appl. Meteor.,* **44,** 1544–1562.

——, S. Y. Matrosov, and T. Uttal, 2006: Arctic mixed-phase cloud properties derived from surface-based sensors at SHEBA. *J. Atmos. Sci.,* **63,** 697–711.

——, and Coauthors, 2008: A focus on mixed-phase clouds: The status of ground-based observations. *Bull. Amer. Meteor. Soc.,* **89,** 1549–1562.

——, V. P. Walden, E. Eloranta, T. Uttal, J. R. Campbell, S. M. Startweather, and M. Shiobara, 2011: Clouds at Arctic atmospheric observatories. Part I: Occurrence and macrophysical properties. *J. Appl. Meteor. Climatol.,* **50,** 626–644.

Sirios, A., and L. A. Barrie, 1999: Arctic lower tropospheric aerosol trends and composition at Alert, Canada: 1980–1995. *J. Geophys. Res.,* **104,** 11 599–11 618.

Solomon, S., and Coauthors, 2007: Technical summary. *Climate Change 2007: The Physical Science Basis,* S. Solomon et al., Eds., Cambridge University Press, 19–92.

Stamnes, K., S.-C. Tsay, W. Wiscombe, and K. Jayaweera, 1988: Numerically stable algorithm for discrete-ordinate-method

radiative transfer in multiple scattering and emitting layered media. *Appl. Opt.,* **27,** 2502–2509.

Stramler, K., A. D. Del Genio, and W. B. Rossow, 2011: Synoptically driven Arctic winter states. *J. Climate,* **24,** 1747–1762.

Sun, Z., and K. Shine, 1994: Studies of the radiative properties of ice and mixed-phase clouds. *Quart. J. Roy. Meteor. Soc.,* **120,** 111–137.

Turner, D. D., 2003: Microphysical properties of single and mixed-phase Arctic clouds derived from ground-based AERI observations. Ph.D. thesis, University of Wisconsin—Madison, 167 pp. [Available online at http://www.ssec.wisc.edu/library/turnerdissertation.pdf.]

——, 2005: Arctic mixed-phase cloud properties from AERI lidar observations: Algorithm and results from SHEBA. *J. Appl. Meteor.,* **44,** 427–443.

——, 2007: Improved ground-based liquid water path retrievals using combined infrared and microwave approach. *J. Geophys. Res.,* **112,** D15204, doi:10.1029/2007/JD008530.

——, and E. W. Eloranta, 2008: Validating mixed-phase cloud optical depth retrieved from infrared observations with high spectral resolution lidar. *IEEE Geosci. Remote Sens. Lett.,* **5,** 285–288.

——, B. M. Lesht, S. A. Clough, J. C. Liljegren, H. E. Revercomb, and D. C. Tobin, 2003: Dry bias and variability in Vaisala RS80-H radiosondes: The ARM experience. *J. Atmos. Oceanic Technol.,* **20,** 117–132.

——, R. O. Knuteson, H. E. Revercomb, C. Lo, and R. G. Dedecker, 2006: Noise reduction of Atmospheric Emitted Radiance Interferometer (AERI) observations using principal component analysis. *J. Atmos. Oceanic Technol.,* **23,** 1223–1238.

——, S. A. Clough, J. C. Liljegren, E. E. Clothiaux, K. Cady-Pereira, and K. L. Gaustad, 2007: Retrieving liquid water path and precipitable water vapor from Atmospheric Radiation Measurement (ARM) microwave radiometers. *IEEE Trans. Geosci. Remote Sens.,* **45,** 3680–3690.

Twomey, S., 1977: The influence of pollution on the shortwave albedo of clouds. *J. Atmos. Sci.,* **34,** 1149–1152.

Uttal, T., and Coauthors, 2002: Surface heat budget of the Arctic Ocean. *Bull. Amer. Meteor. Soc.,* **83,** 255–275.

Vavrus, S., 2004: The impact of cloud feedbacks on Arctic climate under greenhouse forcing. *J. Climate,* **17,** 603–615.

Verlinde, J., and Coauthors, 2007: The Mixed-Phase Arctic Cloud Experiment. *Bull. Amer. Meteor. Soc.,* **88,** 205–221.

Vogelmann, A. M., and Coauthors, 2012: RACORO extended-term aircraft observations of boundary layer clouds. *Bull. Amer. Meteor. Soc.,* **93,** 861–878.

Wang, M., and J. E. Overland, 2009: A sea ice free summer Arctic within 30 years? *Geophys. Res. Lett.,* **36,** L0752, doi:10.1029/2009GL037820.

Wang, X., and J. R. Key, 2005: Arctic surface, cloud, and radiation properties based on the AVHRR Polar Pathfinder Dataset: Part II: Recent trends. *J. Climate,* **18,** 2575–2593.

Wang, Z., K. Sassen, D. N. Whiteman, and B. B. Demoz, 2004: Studying altocumulus with ice virga using ground-based active and passive remote sensors. *J. Appl. Meteor.,* **43,** 449–460.

Zhao, C., and Coauthors, 2012: Toward understanding of differences in current cloud retrievals of ARM ground-based measurements. *J. Geophys. Res.,* **117,** D10206, doi:10.1029/2011JD016792.